Velocity slice imaging for dissociative electron attachment

Dhananjay Nandi, Vaibhav S. Prabhudesai, and E. Krishnakumar[a)]
Tata Institute of Fundamental Research, Homi Bhabha Road, Colaba, Mumbai 400005, India

A. Chatterjee
Nuclear Physics Division, Bhabha Atomic Research Centre, Mumbai, 400 085, India

(Received 1 November 2004; accepted 8 March 2005; published online 26 April 2005)

A velocity slice imaging method is developed for measuring the angular distribution of fragment negative ions arising from dissociative electron attachment (DEA) to molecules. A low energy pulsed electron gun, a pulsed field ion extraction, and a two-dimensional position sensitive detector consisting of microchannel plates and a wedge-and-strip anode are used for this purpose. Detection and storage of each ion separately for its position and flight time allows analysis of the data offline for any given time slice, without resorting to pulsing the detector bias. The performance of the system is evaluated by measuring the angular distribution of O^- from O_2 and comparing it with existing data obtained using conventional technique. The capability of this technique in obtaining forward and backward angular distribution data is shown to have helped in resolving one of the existing problems in the electron scattering on O_2. © *2005 American Institute of Physics.*
[DOI: 10.1063/1.1899404]

I. INTRODUCTION

A variety of charged particle imaging techniques have been used in atomic collision studies based on the time-of-flight technique.[1] Measurement of all three momentum components including multiparticle coincidence has been achieved in several of these experiments on ion-atom/molecule collisions and photoionization and intense field ionization of atoms and molecules.[2–4] Velocity map imaging is another technique used in photodissociation,[5] photodetachment,[6] and photoionization experiments[7] to measure the two momentum components in a given plane of interest. Though the velocity map imaging originally developed by Eppink and Parker necessitates the use of a suitable inversion procedure to determine the velocity vectors of the products,[5] recent developments in this area allow the direct mapping of the velocity vectors without an inversion procedure.[8,9] In these experiments, the Newton spheres of the product species are allowed to expand in all three directions while they are transported to the detector unlike the original technique[5] in which they were allowed to expand only in the plane parallel to the two-dimensional detector. From a given Newton sphere, the particular slice which had no velocity component initially in the direction perpendicular to the detector plane is selectively detected by allowing the detector to be active only in a given narrow time interval with appropriate pulsing of detector bias voltage. A time-resolved event counting based on a double exposure charge-coupled device (CCD) camera has recently been reported to obtain two-dimensional velocity components as a function of time with 1 ns resolution.[10]

In all these charged particle imaging techniques, the particles are generated using neutral beams, photons, or swift projectiles such that imaging could be carried out by applying suitable electric or electric + magnetic fields to get optimum performance. Here we describe the use of the velocity map imaging for low energy electron collision experiments.

Dissociative ionization and dissociative electron attachment (DEA) are important processes occurring in electron-molecule collisions. The dynamics of these processes could be obtained only from the kinetic energies and angular distribution of the products. The angular distribution measurements are particularly important for the case of DEA, due to the selection rules, which connects the states of the neutral molecule to the negative ion resonant states and the orientation of the neutral molecule with respect to the incoming electron momentum vector.[11] Thus the angular distribution contains information on the symmetry of the negative ion state and the angular momentum of the electron that was captured.[12] Angular distribution measurements in DEA have been reported for several molecules using the conventional method of physically moving the detector with respect to the electron beam direction.[13–16] This method has an angular range of at best 20 to 160 deg, due to the geometrical limitations. Moreover the sequential nature of the measurement makes it time consuming and prone to systematic errors. Our recent efforts toward carrying out electron collisions from excited molecules necessitated us to work with pulsed electron beams of poor duty cycles and very small target molecule densities.[17,18] We found that the suitable implementation of a velocity map imaging allowed us to overcome these limitations and obtain angular information in full 0 to 180 deg range on either side.

II. SELECTION OF THE IMAGING SCHEME

The DEA in molecules occur right from zero electron energies, depending on the molecules. The electron beams

[a)]Electronic mail: ekkumar@tifr.res.in

are produced generally using thermionic emission from heated filaments and the electrons being guided by a magnetic field. These guns could provide currents in the range of tens of microamperes and in nanoamperes after monochromatization in the dc mode of operation. If the experiments are to be done on excited molecules, the electron gun has to be operated in the pulsed mode with repetition rates matching with the lasers used for preparing the molecules in the excited states, so that the signal from the excited states of small number densities are not lost in the signal from the ground state molecules. The pulsed mode of operation also provides a way of applying sufficiently strong ion extraction fields to enable their complete extraction and mass analysis, irrespective of their kinetic energies. With the current technology, the repetition rates of lasers with enough power in the ultraviolet are in the 100 Hz region. In order to obtain reasonable current at such low repetition rates, the pulse width of the gun should be several hundred nanoseconds. This type of pulse widths is much larger than the laser pulse widths used in photodissociation or photoionization experiments where velocity map imaging has been traditionally employed. In other collision experiments employing three-dimensional momentum spectrometers the time resolution needed is provided by coincidence measurements. We realized that the constraint related to the fairly large pulse width in electron beams could be overcome if we adapt the velocity slice imaging developed by Gebhardt and coworkers.[8] In this technique the cloud of ions were allowed to expand for a while after the ionizing laser pulse, before they were extracted by a pulsed electric field. This technique eminently suited our purpose since we had an electron beam of fairly large pulse width and the electric field could be applied only after the electron pulse to prevent it from affecting the low energy electron beam. However, we have used a different approach to time slice the Newton spheres by recording each event separately and carrying out offline analysis instead of pulsing the detector bias.

III. EXPERIMENTAL ARRANGEMENT

The schematic of the experimental arrangement is given in Fig. 1. It contained a magnetically collimated and pulsed electron gun, a Faraday cup to measure the current, an effusive molecular beam, a time-of-flight velocity map imaging electrode system, and a two-dimensional position sensitive detector with associated data acquisition system. The experiment was carried out in a vacuum chamber, which was pumped down to few times 10^{-9} Torr using a 2000 l/s turbo pump and scroll pump arrangement.

A. Electron gun and the molecular beam

A gun in the Pierce geometry was used to produce the electron beam with a heated tungsten filament acting as the source of electrons. The beam was collimated by a magnetic field produced by a set of Helmholtz coils kept outside the vacuum chamber. The typical magnetic field used in the present experiment was 50 G. The gun was pulsed by applying a negative bias on the electrode in front of the Pierce element with respect to the filament and overriding it with a positive pulse of appropriate width and amplitude and subnanosecond rise time. This pulse was derived from a pulse generator, which acted as the source for all timing pulses necessary for the experiment. After going through the interaction region, the electron beam was collected in a Faraday cup.

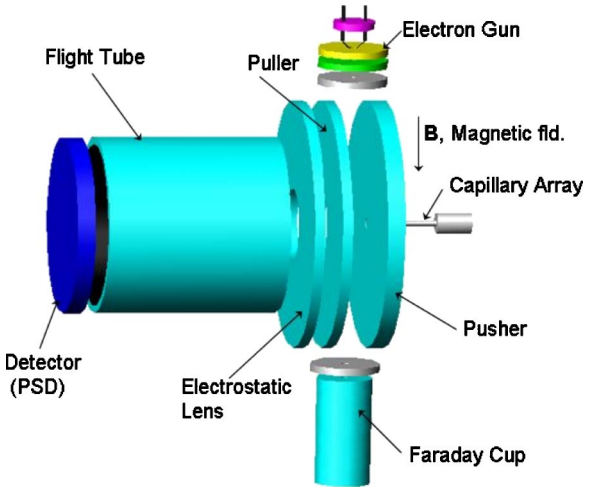

FIG. 1. (Color online) Schematic of the experimental setup.

The width of the electron gun pulse could be varied from 25 ns to 1 μs. The height of the pulses was a few volts. In the present experiment the repetition rate was kept at about 20 kHz, with a time averaged current of a few nanoamperes (1–2 nA) at a pulse width of 200 ns. The energy resolution of the electron beam was about 0.5 eV.

The molecular target was provided by an effusive beam from a capillary array, which was mounted on the pusher plate of the ion extraction arrangement without being allowed to stick out into the interaction region. The axis of the molecular beam was along the axis of the time-of-flight setup. The capillary array was held at the same potential as the pusher plate.

B. Ion optics for velocity map imaging

The ion optics for the velocity map imaging is shown in Fig. 2 and is very similar to what has been used in Ref. 8, except that we avoided using any wire mesh. It consisted of a three-electrode arrangement and a 50 mm long flight tube.

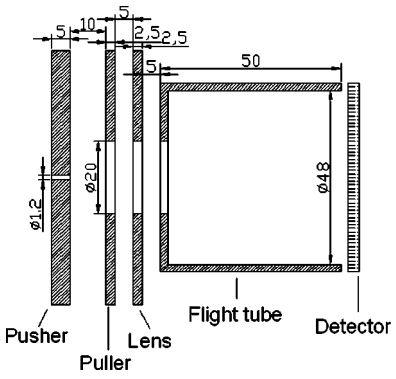

FIG. 2. Scaled schematic of the ion optics for velocity map imaging (all dimensions are in millimeters).

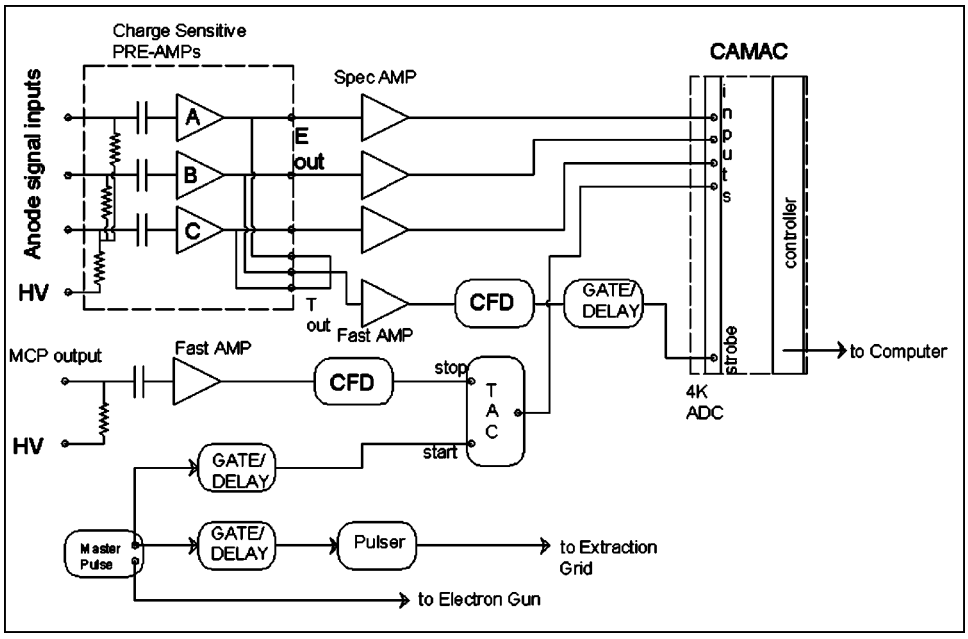

FIG. 3. Block diagram for the data acquisition system.

The assembly was mounted horizontally, with its axis parallel to the molecular beam direction and perpendicular to the electron beam. The three electrodes were made of 70 mm diameter oxygen-free high conductivity copper plates with a coat of colloidal graphite. The flight tube had an inner diameter of 48 mm and was made of nonmagnetic stainless steel. The first of the three electrodes (pusher electrode) had a central hole of 1.2 mm diameter in order to introduce the effusive molecular beam at right angles to the electron beam at the interaction region. The second electrode (puller electrode) and the third electrode (lens) had 20 mm diameter apertures at their centers. The flight tube had 20 mm entrance aperture and 50 mm diameter exit aperture towards the detector. The separation between the pusher and puller electrodes was 10 mm whereas the lens electrode was separated by 5 mm gaps on either side. During the experiment, the optimum voltages for the best velocity map imaging for O^- ions from O_2 at an electron energy of 8 eV was determined by adjusting the voltage ratios applied to the pusher, the lens electrode, and the flight tube with the puller electrode at ground potential. The voltages thus determined were found to be pretty close to the values obtained using ion trajectory calculations done prior to the experiments.

The ion trajectory simulations were carried out for ions of a relatively large kinetic energy of 2 eV. The size of the ion source in the present case was limited by the size of the molecular beam as the capillary array was 5 mm away from the interaction region. The electron gun had apertures less than 1 mm in size and was collimated by the magnetic field. For reasonable electron beam current, we had to operate the gun with about 100–200 ns pulse width. For an electron gun pulse width of 200 ns and an extraction pulse delay of 200 ns (so that necessary blooming of the ion cloud occurs for time slicing purpose) the O^- ions of 2 eV energy spread out to a maximum distance of 2 mm in all directions for isotropic distribution. Since we needed to keep the interaction region field free during the electron pulse and we were not using any grids to prevent field leakage, we had to keep the overall voltages as low as possible. For a 40 mm diameter detector, this necessitated using relatively short flight tube. With these constraints and a source volume of diameter 4 mm, we optimized the voltages for optimum velocity map imaging conditions, using ion trajectory calculations. We found the following voltages to be optimum: pusher electrode at -22 V, puller electrode at ground potential, lens electrode at $+26$ V, flight tube at $+130$ V, and front end of multichannel plate (MCP) detector at $+190$ V. All the above voltages were taken as dc voltages in our calculations. In real experiments, we used a pulsed (pulse height: -22 V and width: 1 μs) extraction voltage at pusher electrode and on the other electrodes we used dc voltages. In actual measurements we tried to optimize the performance of the velocity map imaging by changing the voltage ratios obtained from the calculation, but did not find much deviation from the calculated values.

C. Position sensitive detector and data acquisition system

We used a *Z* stack of three MCPs of 48 mm active area as the detector. A wedge-and-strip (W&S) anode was used for obtaining the two-dimensional position information.[19] The schematic of the data acquisition system is shown in Fig. 3. Signals from the W & S anode were capacitively coupled to a set of charge-sensitive preamplifiers (CASTA, Roent-Dek). These were amplified further using spectroscopy amplifiers before being fed into a four-channel computer automated measurement and control (CAMAC)-based nuclear analog-to-digital converter (ADC) (CM60, 4K). The ADC had a conversion time of 3.5 μs per input and measured the peak of the positive input signals. The conversion was initiated by external fast nuclear instrumentation module (NIM) strobe input, which had been generated from the time outputs of the preamplifiers. A gate width (which could be adjusted from 100 ns to 5 μs) of about 3 μs was generated, triggered by this external strobe signal. The delay between the strobe pulse and the gate was kept ~250 ns. During the gate width

the peak value of all four inputs were detected and stretched, the peak position of all inputs were within the gate signal. A fast timing amplifier was used to amplify the timing signal derived from the rear end of the MCP *Z* stack and after discrimination; this signal was used as a STOP pulse of time-to-amplitude converter for the time-of-flight determination. The ADC and the controller module were housed in a CAMAC mini crate (Kinetic System, Model: 1507) connected to a peripheral componant interface (PCI) card via a CC 2000 crate controller. This crate controller and the ADC mentioned above were supplied by Electronics Division, Bhabha Atomic Research Centre, Mumbai. Once the charge signals had been digitized, the impact positions of the ions onto the detector were calculated from simple standard expressions

$$X = S/(S + W + M),$$

$$Y = W/(S + W + M).$$

S, *W*, and *M* refer to the charge signals measured from strip, wedge, and meander respectively.

The data were acquired using the program LAMPS[20,21] running on Linux operating system. The positions *X*, *Y* were defined as pseudoparameters in LAMPS and the position spectra were displayed online. The data were collected in list mode and the same program was used in the offline analysis as described below.

IV. EXPERIMENTS ON O_2

Our system was tested for its performance by studying the formation of O^- from O_2 by DEA. The formation of O^- from O_2 is known to appear as a broad peak centered at 6.5 eV.[22,23] These ions are also formed with considerable kinetic energy, which have been measured by several workers.[24,25] The angular distribution of O^- from O_2 has also been measured at a number of electron energies around the resonance peak[13] using the conventional turn-table arrangement. In the present measurements, we first obtained the ion yield curve using the voltage conditions appropriate for velocity mapping and by selecting the time window corresponding to O^- ions. The position of the peak obtained from the ion yield curve was used to calibrate the energy scale. The ion yield curve is shown in Fig. 4. The velocity map images were taken at three different electron energies, at the energy corresponding to the peak in the ion yield curve, and 1.5 eV from the peak on either side. A typical time-of-flight (TOF) spectrum of O^- at the 6.5 eV is shown in Fig. 5. The ions ejected towards the flight tube direction appear as a clear peak in the TOF spectrum followed by a slight dip in the center and a relatively broader peak indicating the ions ejected away from the flight tube direction. Since there was no clear-cut minimum in the TOF signal, which could be directly related to the ions ejected at 90 deg to the flight tube direction, we analyzed the list mode data for two-dimensional distribution with time slices of 50 ns each between the two peaks of the TOF distribution. This gave us time-sliced velocity map images with annular distributions of the type shown in Fig. 6. From these images we picked the one with largest diameter since ions ejected at 90 deg with respect to the flight tube axis would have maximum range in the detector plane. We found that within a 200 ns time range in the central section of the TOF distribution, these rings were similar within statistical errors. The time-sliced images obtained at three incident electron energies along with the corresponding three-dimensional plots with intensity as the third axis is shown in Fig. 6. The direction of the electron beam for the images on the left panel is vertically down. The intensity distribution along the radius of these patterns should provide information on the kinetic energy distributions of the ions. The kinetic energy of the ions should be proportional to square of the radius of the annular patterns if there is no electrostatic lens along the flight path. Since we employed such a lens in the velocity mapping, the distribution was found not to follow this relationship from a comparison of the data taken at different electron energies. Thus in order to obtain the kinetic energy data from these images, one may need to resort to some calibration procedure. However, the data clearly show the angular distribution of the ions with very good resolution. The uniformity of the data in both the halves about the electron beam direction emphasizes the absence of any systematic errors in the imaging process, including efficiency variation on the detector surface that

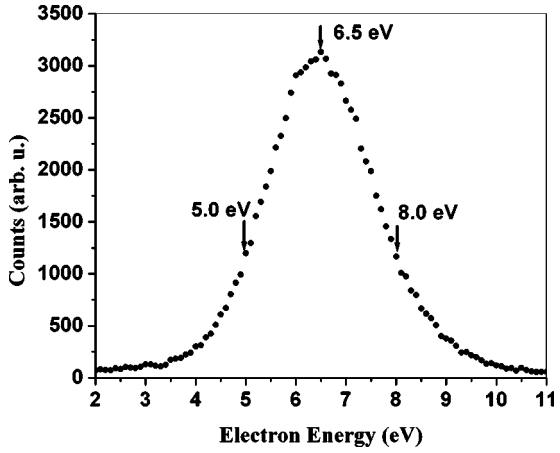

FIG. 4. Ion yield curve for the formation of O^- from O_2 by DEA. The arrows represent the electron energies where the velocity map images are reported.

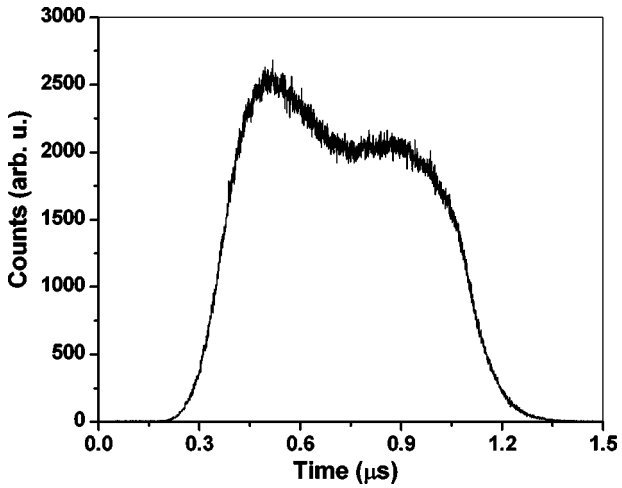

FIG. 5. Time-of-flight mass spectrum of O^- from O_2 taken at 6.5 eV.

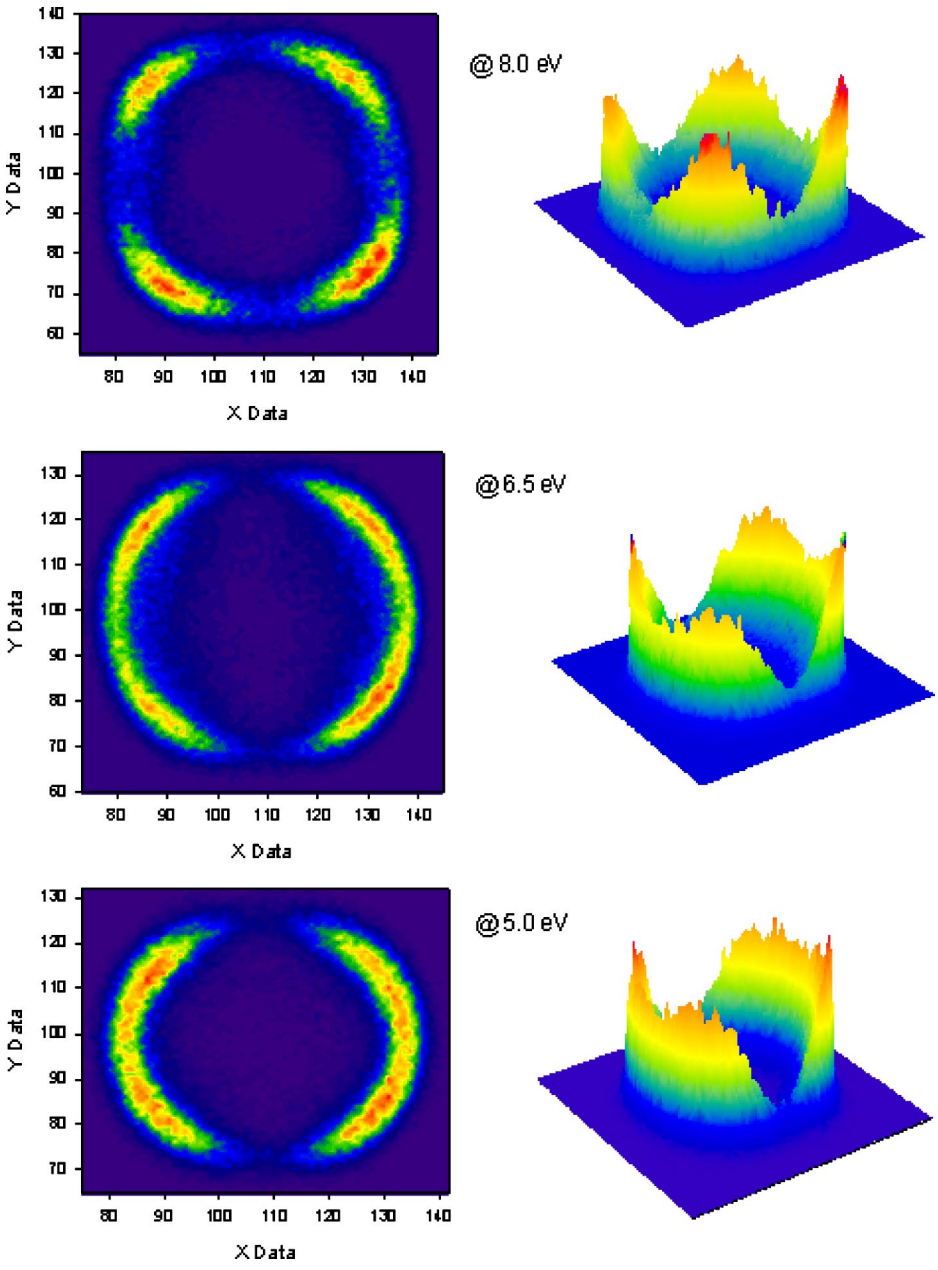

FIG. 6. (Color online) Time sliced velocity map images of O^- from O_2 at three different electron energies. The left panel shows a two-dimensional pattern we obtained after time slicing. The electron beam direction is vertically down. The right panel shows the corresponding three-dimensional distribution with intensity as the *z* axis. These distributions have been rotated through 35 deg in the counter clockwise direction.

may arise due to the relatively small acceleration (about 200 V) the ions underwent before they struck the detector.

The angular distribution of the ions from the time-sliced velocity map images were obtained by integrating over the range of radius over which the annular ring appears and plotting it as a function of the angle. Such plots normalized with respect to the intensities at 90 deg are given in Fig. 7 at three different electron energies and in the angular range from 0 to 360 deg at 2 deg intervals. As expected the angular distributions show almost identical behavior from 0 to 180 deg and 180 to 360 deg at all the three energies, highlighting the quality and consistency of the data. In order to check the performance of the experiment we compared the present data with what is available in the literature,[13] obtained using the conventional method in the range of 20 to 160 deg. This is shown in Fig. 8. Here again the plots are normalized with respect to the intensities at 90 deg. The two sets of data seem to agree with each other very well in the overlapping angular

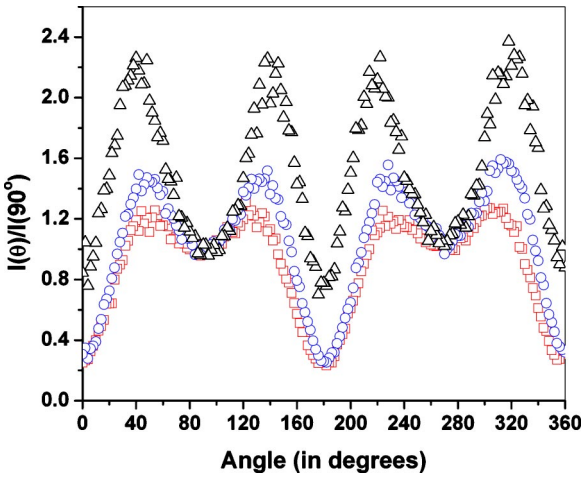

FIG. 7. (Color online) Angular distribution of O^- from O_2. The squares, circles, and triangles are the data at electron energies of 5.0, 6.5, and 8.0 eV respectively.

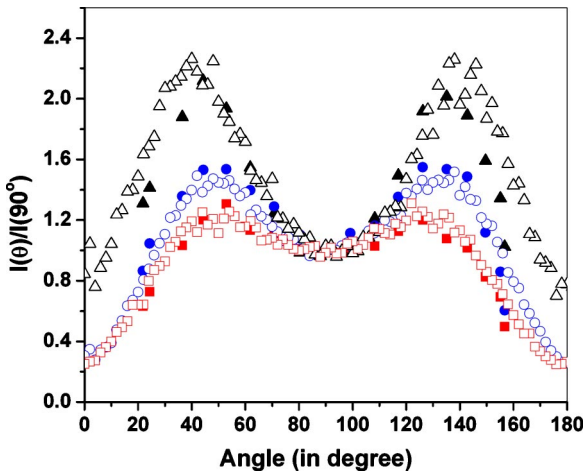

FIG. 8. (Color online) Comparison of the angular distribution of O^- ions from O_2 using velocity map imaging with those obtained using a conventional technique. The open squares, circles, and triangles are the data at electron energies of 5.57, 6.70, and 7.80 eV, respectively, from Ref. 13 and the filled squares, circles, and triangles are the present data at electron energies 5.0, 6.5, and 8.0 eV respectively.

range. Our data used in these figures were collected for the duration of 2–3 h. Apart from the speed of measurement, the present technique provides simultaneous measurement of the angular distribution over the entire range of angles. This eliminates different sources of systematic errors possible in the conventional technique related to the electron beam conditions and maintenance of identical geometric factors. The advantage of covering the entire angular range is brought out very clearly in the nonzero value of the intensity in the forward and backward directions seen in the O^- data as discussed below.

As mentioned in Sec. I angular distribution is dependent on the symmetry of the resonant state and the angular momenta of the attached electrons. For a given electron incident momentum k, the ion intensity I at the angular coordinates (θ,φ) is given by the expression[12]

$$I(k,\theta,\phi)=\sum_{|\mu|}\left|\sum_{l=|\mu|}^{\alpha} a_{l\mu}(k)Y_{l\mu}(\theta,\phi)\right|^2.$$

Here, $a_{l\mu}(\mathrm{k})$ is energy dependent expansion coefficient and $Y_{l\mu}(\theta,\varphi)$ are the spherical harmonics with $\mu=\Lambda_f-|\Lambda_i|$ and $l\geqslant|\mu|$.

The data from the previous measurements appeared to fit well with the functional form $|\sin\theta+5\beta'\sin\theta\cos^2\theta|^2$ for specific values of β'.[13] This functional form corresponds to a single resonant state of Π_u characteristics. According to this functional form the angular distribution should have zero intensity in the forward and backward directions. However, recent electron inelastic scattering experiments[26] have shown that there is a broad peak centered at 9 eV and in the range of 6 to 16 eV in the cross section for excitation of vibrational levels of the ground electronic state of O_2. For incident electron energy of 9 eV, it was found that vibrational levels all the way fairly close to the dissociation limit of O_2 ground state are excited[26] and it was suggested that this is due to resonant scattering from the $^4\Sigma_u^-$ state. Further inelastic scattering experiments and theoretical calculations have shown the existence of the $^4\Sigma_u^-$ state.[27] The vibrational excitation data show that this state has sufficiently long autodetachment lifetime to manifest in the DEA channel also. If the $^4\Sigma_u^-$ state contribute to the DEA, the angular distribution of O^- should have finite intensity in the forward and backward directions. Since the previous angular distribution measurements did not indicate the presence of the $^4\Sigma_u^-$ state, it has remained a puzzle. However, our measurements clearly show nonzero intensity in the forward and backward directions. It is also seen that the forward and backward cross sections increase as the electron energy is increased. We find that a fit using both $^2\Pi_u$ and $^4\Sigma_u^-$ states agree very well with our data. A detailed analysis of this will be presented elsewhere. What we wish to point out here is the importance of the measurements in the forward and backward directions in this type of collision experiments. Though our data are in agreement with the previous reports in the range of angle (20 to 160 deg) where there is overlap, the conclusions from the two set of measurements are different. This shows the importance of having data in the entire angular range, particularly in the forward and backward directions.

V. PERFORMANCE ANALYSIS

As discussed in the previous section, the present experiment seems to work quite well based on the comparison with the previously available data. However we experimented with various parameters used in the experiment in order to test their robustness and range of validity. These are discussed below.

A. Electron gun pulse width and extraction delay

Since the ions were extracted from the interaction region after some delay depending on the electron beam pulse width and the delay in the extraction pulse, the ion cloud bloomed in the interaction region depending on the initial velocity. Since we were interested in keeping as large an electron pulse width as possible for experiments involving low target densities or low cross sections, we investigated the performance of the system by measuring the time-sliced velocity map image as a function of these two parameters, while keeping the other constant. We found that we got satisfactory performance for a combined pulse width and extraction pulse delay up to 700 ns in the case of O^- from O_2 for the combination of voltages we employed. Beyond this time the performance appeared to deteriorate. Since the volume to which the ions spread depends on their velocity, what we observed may not be applicable to all cases, but could be taken as a general guideline. The optimization will have to be carried out according to the situation. As stated earlier, the data presented here were collected with an electron gun pulse width and delay of 200 ns each.

B. Effect of the magnetic field

In our measurements we used a homogeneous magnetic field in order to collimate the electron beam. The ions were extracted and collected perpendicular to the magnetic field direction. The Lorentz force acting on the ions was expected to affect their trajectories and their subsequent positions on

the detector depending on the magnetic field strength. It was found that by changing the magnetic field strength from 25 to 100 G and its direction, the whole image was shifting its position on the detector without changing the shape of the image. The observed shift was found to be consistent with the strength and direction of the field and the ion mass and velocity. The data presented here were collected with a magnetic field of about 50 G.

Another important aspect of the presence of the magnetic field in the present experiment was its effect on the angular resolution of the experiment. The limiting angular resolution (θ) is related to the transverse energy spread (ΔE_{trans}) in the electron beam and its longitudinal energy (E_{long}) through the relation

$$\theta = \tan^{-1}\sqrt{\frac{\Delta E_{\text{tran}}}{E_{\text{long}}}}.$$

This was an aspect we had been quite concerned about right from the conceptual stage of the experiment. If one considers all the observed energy spread of 0.5 eV in our experiment is equally contributed by the transverse and longitudinal contributions, at the electron energy of 5 eV, the angular resolution would be about ± 17.5 deg and at lower electron energies this could be worse. Apparently, the present measurements on O^- from O_2 at 5 eV do not show any effect due to such poor angular resolution as the present data appears to be in excellent agreement with that reported with an angular resolution of ± 1.2 deg.[13] This may be due to the fact that most of the contribution for the energy spread could be arising from the longitudinal contribution. There is no clear cut way of measuring the transverse and longitudinal energy spread separately. An estimate of the upper limit of the transverse spread may be determined by carrying out a retarding potential energy measurement by either measuring the electron beam current or the DEA signal. Early measurements using retarding potential measurements with similar electron guns in the presence of a magnetic field have shown that the energy resolution could be as low as 0.1 eV.[28] We carried out an analysis of the angular spread on the data due to the transverse energy spread of the electron beam assuming a Gaussian distribution of energy and taking the functional form corresponding to contributions from both the $^2\Pi_u$ and the $^4\Sigma_u^-$ states. For a given half-width of the energy distribution, the angular spread was calculated at each point in the energy and using appropriate weight, it was convolved with the above functional form. This was compared with our measured data and the χ^2 were evaluated. The process was repeated with different half-widths for the transverse electron energy spread until the χ^2 reached minimum. We found that the transverse energy spread thus obtained could have a maximum value of 80 meV. The corresponding angular spread at 5 eV is about 7 deg. This analysis shows that the transverse energy spread is indeed small as seen from the previous retarding potential measurements. We also found that even the 7 deg angular spread seems to have a relatively small effect on the accuracy of determining the angular distribution as compared to the statistical errors, primarily due to the slow varying nature of the angular distribution function in the present case. In general, the angular distributions arising from DEA are slow varying functions as the process is generally dominated by the capture of electrons with smaller angular momentum. Hence the measurements may not demand extremely high angular resolution. However, the angular resolution problem has to be kept in mind while using this technique for magnetically collimated low energy electron beams. The angular resolution could be improved with improvement in electron energy resolution.

Very recently, a comparative study of three different slicing methods for velocity map imaging (VMI) has been reported for photodissociation experiments,[29] in which it is pointed out that the use of a grid on the puller electrode and application of delayed extraction by pulsing both the pusher and puller electrodes, leads to more reliable kinetic energy data. Though we have tried to implement it, our efforts have not succeeded so far due to electrical interference at the wedge-and-strip anode used to record position information. Unlike a CCD camera based position readout, which is used in the above photodissociation experiments, the present system makes use of charge integrating amplifiers and hence is very susceptible to electrical noise.

ACKNOWLEDGMENTS

The authors acknowledge with thanks V. M. Nanal and K. Ramachandran for their help in setting up the data acquisition system. V.S.P. and D.N. acknowledge the TIFR Alumni Association scholarship from the TIFR Endowment fund.

[1] *Imaging in Molecular Dynamics*, edited by Benjamin Whitaker (Cambridge University, Cambridge, England, 2003).
[2] R. Dörner, V. Mergel, L. Spielberger, M. Achler, Kh. Kayyat, T. Vogt, H. Bräuning, O. Jagutzki, T. Weber, J. Ullrich, R. Moshammer, M. Unverzagt, W. Schmitt, H. Khemliche, M. H. Prior, C. L. Cocke, J. Feagin, R. E. Olson, and H. Schmidt-Böcking, Nucl. Instrum. Methods Phys. Res. B **124**, 225 (1997).
[3] Z. Amitay and D. Zajfman, Rev. Sci. Instrum. **68**, 1387 (1997).
[4] H. Helm, N. Bjerre, M. J. Dyer, D. L. Huestis, and M. Saeed, Phys. Rev. Lett. **70**, 3221 (1993).
[5] A. Eppink and D. H. Parker, Rev. Sci. Instrum. **68**, 3477 (1997).
[6] E. Surber and A. Sanov, Phys. Rev. Lett. **90**, 093001 (2003).
[7] B. Baguenard, J. B. Wills, F. Pagliarulo, F. Lépine, B. Climen, M. Barbaire, C. Clavier, M. A. Lebeault, and C. Bordas, Rev. Sci. Instrum. **75**, 324 (2004).
[8] C. R. Gebhardt, T. P. Rakitzis, P. C. Samartzis, V. Ladopoulos, and T. N. Kitsopoulos, Rev. Sci. Instrum. **72**, 3848 (2001).
[9] D. Townsend, M. P. Minitti, and A. G. Suits, Rev. Sci. Instrum. **74**, 2530 (2003).
[10] L. Dinu, A. T. J. B. Eppink, F. Rosca-Pruna, H. L. Offerhaus, W. J. van der Zande, and M. J. J. Vrakking, Rev. Sci. Instrum. **73**, 4206 (2002).
[11] G. H. Dunn, Phys. Rev. Lett. **8**, 62 (1962).
[12] T. F. O'Malley and H. S. Taylor, Phys. Rev. **176**, 207 (1968).
[13] R. J. Van Brunt and L. J. Kieffer, Phys. Rev. A **2**, 1899 (1970).
[14] R. J. Van Brunt and L. J. Kieffer, Phys. Rev. A **10**, 1633 (1974).
[15] I. Cadez, M. Tronc, and R. I. Hall, J. Phys. B **8**, L73 (1975).
[16] M. Tronc, F. Fiquet-Fayard, C. Schermann, and R. I. Hall, J. Phys. B **10**, L459 (1977).
[17] E. Krishnakumar, S. V. K. Kumar, S. A. Rangawala, and S. K. Mitra, Phys. Rev. A **56**, 1945 (1997).
[18] S. A. Rangawala, S. V. K. Kumar, and E. Krishnakumar, Phys. Rev. A **64**, 012707 (2001).
[19] C. Martin, P. Jelinsky, M. Lampton, R. F. Malina, and H. O. Anger, Rev. Sci. Instrum. **52**, 1067 (1981).
[20] A. Chatterjee, http://www.tifr.res.in/~pell/lamps.html
[21] A. Chatterjee, S. Kamerkar, A. K. Jethra, S. Padmini, M. P. Diwakar, S. S. Pande, and M. D. Ghodgaonkar, Pramana, J. Phys. **57**, 135 (2001).

[22] H. S. W. Massey, *Negative Ions* (Cambridge University, Cambridge, England, 1976).
[23] D. Rapp and D. D. Briglia, J. Chem. Phys. **43**, 1480 (1965).
[24] P. N. Chantry and G. J. Schulz, Phys. Rev. **156**, 134 (1967).
[25] T. Oster, A. Kühn, and E. Illenberger, Int. J. Mass Spectrom. Ion Processes **89**, 1 (1989).
[26] M. Allan, J. Phys. B **28**, 5163 (1995).
[27] C. J. Noble, K. Higgins, G. Wőste, P. Duddy, P. G. Burke, P. J. O. Teubner, A. G. Middleton, and M. J. Brunger, Phys. Rev. Lett. **76**, 3534 (1996).
[28] R. E. Fox, W. M. Hickam, D. J. Grove, and T. Kjeldaas, Jr., Rev. Sci. Instrum. **26**, 1101 (1955).
[29] D. A. Chestakov, S. M. Wu, G. Wu, D. Parker, A. T. J. B. Eppink, and T. N. Kistopoulos, J. Phys. Chem. A **108**, 8100 (2004).